D-IMRT verification with a 2D pixel ionization chamber: dosimetric and clinical results in head and neck cancer

(Article begins on next page)

25 April 2024

D-IMRT verification with a 2D pixel ionization chamber: dosimetric and clinical results in head and neck cancer

M Stasi[1], S Giordanengo[2], R Cirio[2], A Boriano[2,3], F Bourhaleb[4], I Cornelius[2], M Donetti[2,5], E Garelli[2,6], I Gomola[7], F Marchetto[2], M Porzio[2,3,8], C J Sanz Freire[2,3,10], A Sardo[2,3,9] and C Peroni[2,3]

[1] Institute for Cancer Research and Treatment (IRCC), Candiolo and A.S.O. Ordine Maurizano, Torino, Italy
[2] Istituto Nazionale di Fisica Nucleare (INFN), Via P. Giuria 1, I-10125 Torino, Italy
[3] Experimental Physics Department, University of Torino, Via P. Giuria 1, I-10125 Torino, Italy
[4] TERA Foundation, Via Puccini 1, I-28100 Novara, Italy
[5] CNAO Foundation, Via Caminadella 16, I-20123 Milano, Italy
[6] ASP, Viale S. Severo 65, I-10125 Torino, Italy
[7] Scanditronix-Wellhöfer, Bahnhofstrasse 5, D-90592 Schwarzenbruck, Germany
[8] A.O. S.S. Antonio, Biagio e C. Arrigo, Via Venezia 16, I-15100 Alessandria, Italy
[9] A.O. O.I.R.M. S. Anna, C. so Spezia 60, I-10126 Torino, Italy

E-mail: cirio@to.infn.it

Abstract

Dynamic intensity-modulated radiotherapy (D-IMRT) using the *sliding-window* technique is currently applied for selected treatments of head and neck cancer at Institute for Cancer Research and Treatment of Candiolo (Turin, Italy). In the present work, a PiXel-segmented ionization Chamber (PXC) has been used for the verification of 19 fields used for four different head and neck cancers. The device consists of a 32×32 matrix of 1024 parallel-plate ionization chambers arranged in a square of 24×24 cm^2 area. Each chamber has 0.4 cm diameter and 0.55 cm height; a distance of 0.75 cm separates the centre of adjacent chambers. The sensitive volume of each single ionization chamber is 0.07 cm^3. Each of the 1024 independent ionization chambers is read out with a custom microelectronics chip.

The output factors in water obtained with the PXC at a depth of 10 cm were compared to other detectors and the maximum difference was 1.9% for field sizes down to 3×3 cm^2. Beam profiles for different field dimensions were measured with the PXC and two other types of ionization chambers; the maximum distance to agreement (DTA) in the 20–80% penumbra region of a 3×3 cm^2 field was 0.09 cm. The leaf speed of the multileaf collimator was varied between 0.07 and 2 cm s^{-1} and the detector response was constant to

better than 0.6%. The behaviour of the PXC was measured while varying the dose rate between 0.21 and 1.21 Gy min^{-1}; the mean difference was 0.50% and the maximum difference was 0.96%. Using fields obtained with an enhanced dynamic wedge and a staircase-like (*step*) IMRT field, the PXC has been tested for simple 1D modulated beams; comparison with film gave a maximum DTA of 0.12 cm. The PXC was then used to check four different IMRT plans for head and neck cancer treatment: cervical chordoma, parotid, ethmoid and skull base. In the comparison of the PXC versus film and PXC versus treatment planning system, the number of pixels with γ parameter $\leqslant 1$ was 97.7% and 97.6%, respectively.

1. Introduction

In recent years, several techniques in beam delivery have been developed in an attempt to obtain precisely conformed dose profiles. Beam intensities can be modified with the use of wedges (static or dynamic) (Khan 1994) and compensator filters (Ellis *et al* 1959). Non-uniform beam intensities can be delivered with a static multileaf collimator (S-MLC) using multiple coplanar or non-coplanar beams to achieve good conformation of dose distributions; moreover, there has been great interest in implementing intensity-modulated radiation therapy (IMRT) in external beam therapy (Ezzell 2003, Purdy 2001, Webb 2000). Dose distributions with improved conformity to the target can be obtained with this technique, leading to a reduced dose to the surrounding healthy tissue and critical organs. The *sliding-window* technique with dynamic multileaf collimators (DMLC) (Convery *et al* 1992, Webb 1989, 1992, 1994) is based on independently moving each leaf pair of a MLC during treatment while the beam is on, to obtain sweeping apertures of variable width across the treatment field. The width of the aperture varies among leaf pairs and for each leaf pair the width is also a function of time.

Sliding-window D-IMRT is currently applied at Institute for Cancer Research and Treatment (IRCC) of Candiolo (Turin, Italy), in particular for the treatment of head and neck cancers.

Due to the complexity of the dynamic IMRT (D-IMRT) techniques, the verification of dose delivery is crucial (Webb 1997) and successful clinical implementation of IMRT requires verifying the consistency between calculated and delivered dose distributions for each patient (Tsai *et al* 1998). Nowadays, one of the most widely used methods for IMRT verification is to compare the dose distribution calculated by the treatment planning system (TPS) in a simple-geometry phantom with the dose distribution measured with films (Ting and Davis 2001, Xing *et al* 1999). If film data are normalized to ionization chamber measurements, the dose distribution can be expressed in absolute values. IMRT verification can also be performed using arrays of silicon diodes (Watts 1998, Zhu *et al* 1997) and matrices of silicon diodes (Jursinic and Nelms 2003, Letourneau *et al* 2004). A check of the beam fluence has also been carried out using 2D beam imaging systems (Li *et al* 2001, Ma *et al* 1998). Electronic portal imaging devices (EPID) are also being used for IMRT verification (Greer and Popescu 2003, Pasma *et al* 1999, Van Esch *et al* 2004, Warkentin *et al* 2003, Zeidan *et al* 2004). An active-matrix flat-panel dosimeter has been recently tested for in-phantom dosimetric measurements (Moran *et al* 2005). All of these detectors have some advantages but, on the other hand, are characterized by some disadvantages. Films have very good spatial resolution and granularity but have to be carefully calibrated (Burch *et al* 1997, Olch 2002, Sykes *et al* 1999, Yeo and Wang 1997, Zhu *et al* 2002) and the measurement is not available in real time.

EPIDs have a good spatial resolution and granularity and provide a real-time measurement; on the other hand, calibration, ageing due to radiation and dead time in electronics read out are to be taken into account. Matrices of detectors (diodes or ionization chambers) have poor granularity. Diodes feature a good spatial resolution, but have the calibration and ageing features of silicon detectors. Ionization chambers have worse spatial resolution than diodes, but provide a direct measurement of the dose, without need for frequent calibration. Indeed, none of these detectors is able to provide every kind of measurement. For example, a matrix, due to the fact that not the whole surface is sensitive, would not allow the correct verification of a plan with very small spikes in dose distribution and would not be able to quantitatively measure the displacement of a single leaf unless appropriate corrections were applied to raw data.

The present work is aimed at verifying the behaviour of a new device for the measurement of head and neck IMRT treatments used in practical clinic at IRCC. The detector is a PiXel-segmented ionization Chamber (PXC); it was designed and built by Torino University and Istituto Nazionale di Fisica Nucleare (INFN). Basic dosimetric properties of the PXC (i.e. detector stability, dose and dose-rate dependence, tissue maximum ratio (TMR)) were described in a previous paper (Amerio *et al* 2004). Recently, Scanditronix-Wellhöfer (Schwarzenbruck, Germany) has commercialized a detector, MatriXX, which is based on the present R&D. PTW (Freiburg, Germany) is also producing a matrix of ionization chambers. The main differences between the two detectors stand in the number of independent ionization chambers (1020 versus 729), their arrangement with respect to the MLC and the dimension of each chamber (4.5 mm diameter $\times$ 5 mm height versus $5 \times 5 \times 5$ mm^3).

2. Materials and methods

Measurements were performed on a Varian Clinac 600 C/D delivering a 6 MV x-ray beam, equipped with Varian Millennium 120-leaf MLC. The 120 leaves are of different sizes: the 40 central leaves are 0.5 cm wide at isocentre and produce a field of up to 20×20 cm^2; the remaining leaves are 1 cm wide, except for the four external ones that are 1.4 cm wide. The maximum obtainable field size is 40×40 cm^2.

Absolute dose calibration of the linac was performed according to the AAPM TG-51 code of practice (Almond *et al* 1999); the measured percent-depth-dose (PDD) was 66.1% for x rays at 10 cm depth in water. Calibration conditions were: a dose rate of 0.01 Gy MU^{-1} at the depth-of-maximum dose (1.5 cm), a source-to-surface distance (SSD) of 100 cm and a field size of 10×10 cm^2. A PTW 30010 cylindrical ionization chamber was used for the calibration. This chamber has a 0.6 cm^3 volume and was calibrated at the German National Laboratory, PTB (Braunschweig, Germany). It was used connected to a PTW Unidos electrometer with a +400 V bias voltage. Beam profiles were measured at 10 cm water-equivalent depth using a water-phantom Wellhöfer Blue-Phantom with two detectors: a cylindrical ionization chamber Wellhöfer IC15 (0.125 cm^3 volume, 0.55 cm internal diameter) and an Exradin (Standard Imaging, Middleton, USA) A16 Micropoint chamber (0.007 cm^3 volume, 0.24 cm internal diameter). IC15 is the detector that is used for the measurement of the data input to the TPS (PDD, relative profiles at five different water-equivalent depths, diagonal profile, output factor (OF)), CadPlan-Helios version 6.3.5 (Varian, Zug, Switzerland).

The two-dimensional dose-measuring detector used in this work is a pixel-segmented ionization chamber. Similar detectors were previously tested on proton (Brusasco *et al* 1997), electron (Belletti *et al* 1999), carbon ion (Bonin *et al* 2004) and x-ray (Amerio *et al* 2004) beams, where they were used as a dosimeter or beam monitor. In this work, results are shown for dosimetry of x-ray IMRT used in four head and neck pathologies. While details of the

chamber construction can be found in Amerio *et al* (2004), a brief description is given in the following. The detector consists of a 32×32 matrix of 1024 parallel-plate ionization chambers arranged in a square of 24×24 cm^2 area. Each chamber has a diameter of 0.4 cm and a height of 0.55 cm; a distance of 0.75 cm separates the centre of adjacent chambers. Due to this geometry, when using the PXC with an MLC with leaves 1 cm wide, each third leave gives a signal that is 13% of the maximum. Tests are under way at present to measure the capability of the PXC to detect errors in leaves' positions. The sensitive volume of each single ionization chamber is 0.07 cm^3. The typical operating voltage is -400 V. The geometry was designed such that all the detectors are symmetric with respect to the axis passing through the central point of the PXC. For this reason, profile plots have points closest to the central axis in the *x*- and *y*-directions at ± 0.375 cm. The PXC can be used as an active detector in a homogeneous phantom by placing solid-water layers in front of the chamber to obtain the desired water-equivalent depths and about 10 cm of solid-water downstream to account for the backscattering effect. Each of the 1024 independent ionization chambers is read out with a custom microelectronics chip, developed at the Torino University and INFN (Bonazzola *et al* 1998). The digital signals are transferred up to 100 m away via two flat cables to a commercial input–output data acquisition board housed in a computer (either laptop or desktop).

The data acquisition programs have been implemented using the National Instruments (Austin, USA) LabVIEW package. The custom microelectronics chip and the data acquisition system have been realized in such a way that the operator can choose, before acquisition is started, how often the 1024 pixels are read. The minimum read-out time for the 1024 pixels is 0.5 ms and it is performed without introducing dead time into the system (Bonazzola *et al* 1998); for the tests presented in the following, the detector was read out once per second. The chips are located close to the sensitive area of the device and are thus in a radiation environment. Several chips were exposed to x ray and neutrons, and their behaviour (dark current, gain, linearity) has been measured (Bourhaleb *et al* 2002) at different values of integrated dose. Change in electronic gain below 1% was found up to 750 Gy of x rays and 4×10^{12} neutrons. With the assumption that outside treatment field the dose is 1% than in the centre, tens of thousands of measurements may be performed with no change in the performances of the read-out electronics.

The relative response among single detectors in multi-detector devices is a problem that has been solved in several different ways in the past; calibration procedures and suitable software are provided by the manufacturers (e.g. SunNuclear (Simon *et al* 2000) and Wellhöfer). We have developed and implemented in LabVIEW a method that sets no constraint on the dimensions and shape of the beam, yet assumes that the beam shape does not change during the three consecutive irradiations needed for the calibration. The method is described in detail in Amerio *et al* (2004) and Garelli (2002). It allows the user to calibrate the area of the PXC needed for the measurement; for example, in the present work, the PXC has been calibrated with a 20×20 cm^2 field. To monitor the stability of the PXC, the calibration constants of the pixels have been measured over a period of 7 months and the change was 1.3% (1σ).

In all the tests described herein, the effective measurement point of the PXC was 100 cm from the accelerator source, at a water-equivalent depth of 5 or 10 cm.

The PXC absolute calibration factor was obtained using the PTW 30010 ionization chamber. The AAPM TG-51 code of practice (Almond *et al* 1999) was used to calculate the reference dose along the central beam axis. The absolute calibration factor of the central pixel was found to be 2.13 ± 0.01 nC Gy^{-1}.

We compared the OF in water at 10 cm depth and 100 cm SSD for a diamond detector PTW 60003 (0.025 cm thickness of sensitive volume) and several ionization chambers:

Table 1. Description of the IMRT fields used at IRCC for head and neck cancer treatments.

Pathology	Number of IMRT fields	Beam angles
Cervical chordoma	7	80, 120, 150, 180, 210, 240, 270
Parotid	4	190, 220, 320, 345
Skull base	4	20, 90, 230, 262
Ethmoid	4	0, 90, 232, 262

Exradin A14 SL (0.009 cm^3 volume, 0.41 cm internal diameter), PTW Pin-Point (0.015 cm^3 volume, 0.2 cm internal diameter), Exradin A16 and Wellhöfer IC15 (that were previously described).

Dose-rate response was measured with the PXC at the water depth of 1.8 cm; the dose rate at the PXC location was in the range 0.21–1.21 Gy min^{-1}, obtained by changing the SSD in the range 90–217.5 cm. In dynamic tests, the behaviour of the PXC was verified with 60° enhanced dynamic wedge (EDW) and a staircase-like (*step*) IMRT field; the PXC measurements were compared with Kodak EDR2 films. A test was also performed to measure the response of the PXC to different speeds of the MLC leaves. The MLC was programmed to move the leaves with a constant speed and to deliver a homogenous dose distribution on an area of 8×11 cm^2 (11 cm along leaf movement) centred on the PXC central pixel. The system was then programmed to deliver different doses (between 0.06 and 8.07 Gy); this resulted in different average speeds of the leaves, in the range 0.07–2.0 cm s^{-1}. The latter value is the highest used for clinical treatments at IRCC.

Films, PXC and TPS were used to check four different IMRT plans in head and neck cancers: cervical chordoma, parotid, ethmoid and skull base. A prescribed dose of 2 Gy at isocentre (ICRU Report 50 1993) was used for each treatment. The field set-up for each plan is shown in table 1. A total of 19 modulated beam fields were verified. Every field was measured with the central beam axis oriented perpendicular to the plane of the PXC and centred on the centre of the PXC. As mentioned previously, the geometry was designed such that all the detectors are symmetric with respect to the axis passing through the central point; thus, the centres of the detectors closest to the central axis are at x and y ± 0.375 cm.

In order to perform the analysis of measured versus calculated dose, the TPS has to compute the dose distribution inside a given solid-water phantom starting from patient-optimized IMRT beams. Each single planned field (including beam parameters and fluence files) can be used to *irradiate* a rectangular homogeneous phantom and thus obtain a *test plan*. The dose was calculated and normalized in such a way that every field of the *test plan* had the same monitor units as the patient-optimized plan. In this study, the dose distribution was calculated at 5 cm water-equivalent depth and SSD 95 cm to simulate IMRT clinical treatment conditions. The fields were then transferred to the accelerator and the phantom was irradiated. X-OMAT V and EDR2 films (Eastman Kodak, Rochester, USA) placed in a water-equivalent phantom (Gammex RMI, USA) were used. Absolute dose was measured with A14 or 30010 chambers. The 2D dose distributions obtained from TPS calculations were compared with films using the RIT315 software (Colorado Springs, USA) interfaced with the VXR-12 Plus film scanner (Vidar, Herndon, USA). An identical set of measurement has been performed replacing film and ionization chambers with the PXC. In this case, the γ-index method (Low *et al* 1998), implemented in LabVIEW-based software developed in house, has been used to compare film, TPS and PXC dose distributions. To compute the γ index, data from the 0.25 cm wide CadPlan grid were linearly interpolated to obtain a 0.05 cm pitch. For the
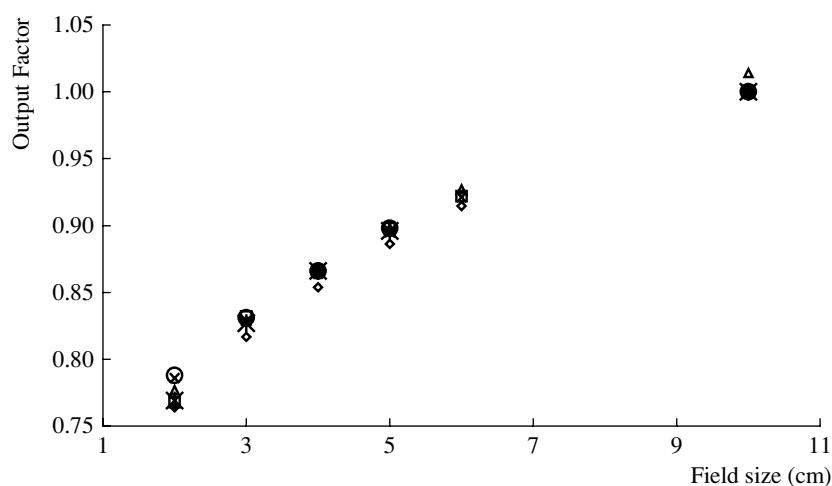
Figure 1. Output factors at 10 cm water depth and SSD of 100 cm, measured with the PXC ($\diamond$), diamond ($\bigcirc$), Pin-Point ($\triangle$), A14SL ($*$), IC15 ($\square$) and A16 ($\times$) ionization chambers. Data were normalized at the 10×10 cm^2 field, except for Pin-Point which was normalized to IC15 at the 5×5 cm^2 field.

Table 2. Output factors at 10 cm water depth and SSD of 100 cm, measured with the PXC, diamond, Pin-Point, A14 SL, IC15 and A16 ionization chambers. Data were normalized at the 10×10 cm^2 field (cf figure 1), except for Pin-Point which was normalized to IC15 at the 5×5 cm^2 field.

Field	PXC	Diamond	Pin-Point	A14 SL	IC15	A16
2×2 cm^2	0.764	0.788	0.777	0.769	0.768	0.786
3×3 cm^2	0.817	0.831	0.829	0.827	0.832	0.829
4×4 cm^2	0.854	0.866	0.867	0.866	0.866	0.864
5×5 cm^2	0.886	0.898	0.898	0.896	0.898	0.895

present analysis, a 0.3 cm distance to agreement (DTA) and 3% dose difference were chosen. AAPM Task Group 53 (Fraass *et al* 1998) suggested these criteria for conformal radiotherapy and they were chosen at IRCC as tolerances for IMRT.

The statistical variation of all PXC measurements was 0.5%; in the plots, this experimental uncertainty is always smaller than symbol dimensions.

3. Results and discussion

Dosimetric characteristics of the PXC such as detector stability, TMR, dose and dose-rate dependence were also studied in a previous paper (Amerio *et al* 2004); the present paper focuses on measurements specific to the use with the clinical IMRT plans used with dynamic MLC at IRCC for head and neck cancers.

3.1. Output factor measurements

Figure 1 and table 2 show a comparison between the OF measured with the PXC, a diamond detector (PTW 60003) and ionization chambers (Wellhöfer IC15, PTW Pin-Point, Exradin A14 SL and Exradin A16 Micropoint). Data were normalized at the 10×10 cm^2 field, except
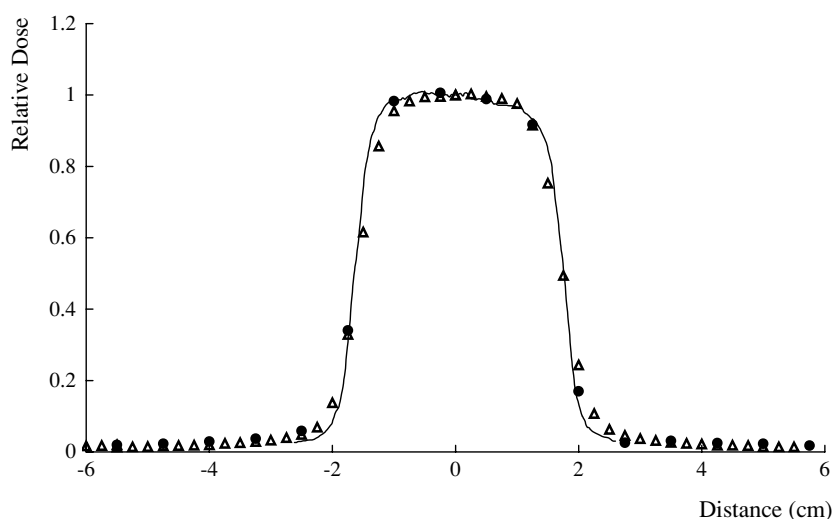
Figure 2. Beam profile of a cross-plane 3×3 cm^2 field measured with the PXC ($\bullet$), IC15 ($\triangle$) and A16 (continuous line).

for Pin-Point which was normalized to IC15 at the 5×5 cm^2 field to take into account its over-response to large fields (Martens *et al* 2000). The OF values obtained with those detectors show a maximum difference of 1.9% for field sizes in the range 3×3 cm^2 to 5×5 cm^2. For a 2×2 cm^2 field, the PXC shows a difference of 3.1% when compared to the diamond detector. The OF was measured using detectors of sizes appropriate for the field dimensions, as it is well known that small fields require a detector with effective dimensions that insure lateral electronic equilibrium (Bucciolini *et al* 2003, Capote *et al* 2004, Leybovich *et al* 2003, Low *et al* 2003, Martens *et al* 2000, 2001, Rustgi and Frye 1995, Stasi *et al* 2003, 2004). Output factor measured with detectors with the smaller volume are close to the measurements with the diamond detector.

3.2. Beam-profile measurements

Figure 2 shows the comparison between the cross-plane 3×3 cm^2 beam profile obtained with A16, IC15 and PXC normalized at the beam central axis. These measurements were also performed for 4×4, 5×5, 6×6, 10×10 and 15×15 cm^2 field sizes.

A16 and PXC data are in good agreement in the radiation field, in the range between 80% and 100% of the maximum (mean difference $0.1 \pm 0.1\%$, maximum difference 2.7%), where the relative response of the 1024 chambers dominates. As previously described, the PXC was calibrated using a method independent from the beam shape and here the effectiveness of the calibration can be appreciated.

In the 20–80% gradient region, the four measurement points of PXC have a maximum DTA of 0.09 cm compared to A16 data. Each one of the 1024 individual chambers in the PXC has a diameter of 0.4 cm and this gives a distorted measurement of large gradients due to a geometric averaging effect, as reported by several authors (Bucciolini *et al* 2003, Capote *et al* 2004, Leybovich *et al* 2003, Low *et al* 2003, Martens *et al* 2000, 2001, Rustgi and Frye 1995, Stasi *et al* 2003, 2004). As expected, this distortion is even worse in the measurements obtained with IC15, which has dimensions larger than PXC (0.6 cm versus 0.4 cm inner diameter).
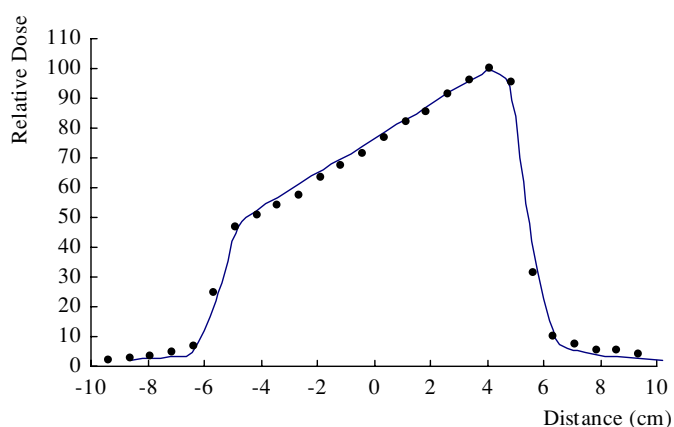
Figure 3. Comparison of film (continuous line) with PXC measurements (●) for the 60° enhanced dynamic wedge.

In the tail region (<20% of the maximum), PXC was compared to IC15 because A16 data were not available at distances larger than ±2.5 cm. However, this is a zone where the dose distribution has no gradient and IC15 data can be safely used as reference. The mean difference was 1.1 ± 0.6% with a maximum of 3.8%. This value is larger than that for the central region of the radiation field (spanning from −1 cm to +1 cm in the field shown in figure 2); on the other hand, there are no regular patterns that would show up if pixels had a capacitive coupling with the tracks that bring the electronic signal from each ionization chamber to the read-out microelectronics chips (cross talk). The increase in the mean value of the difference may be caused by stray radiation interacting with the read-out electronics but this hypothesis is to be further investigated.

3.3. Dose-rate dependence

In order to study the behaviour with dose rate, the PXC response was compared to the values measured with PTW 30010. A mean difference of 0.50 ± 0.31% and a maximum difference of 0.96% at 0.41 Gy min^{-1} have been obtained.

We conclude that the PXC performance in terms of dose-rate dependence is equivalent to that of the reference dosimeter.

The PXC response at low dose has been previously measured (Amerio *et al* 2004) and features a very good linearity, with $R^2 = 1$ from 0.1 Gy to 10 Gy.

3.4. Enhanced dynamic wedge (EDW) and step IMRT measurements

The first simple application of 1D modulated beams, such as EDW, is shown in figure 3. This technique obtains a wedged effect by moving one of the jaws across the field during irradiation. We compared the film measurement versus PXC dose profile at 10 cm water-equivalent depth for 60° EDW and found a mean difference of 2.6 ± 1.9% and a maximum difference of 6.6% in the high-dose zone. In the 20–80% penumbra region, the maximum DTA was 0.12 cm.

A simple *step* IMRT beam was used prior to the verification of clinical IMRT fields. The measured beam profile compared with film is shown in figure 4. In the central zone, where the dose is high, the difference was 1.1 ± 0.7% with a maximum difference of 2.2% in the pixel closest to the high-gradient zone. The single point that fell in the 20–80% high-gradient zone
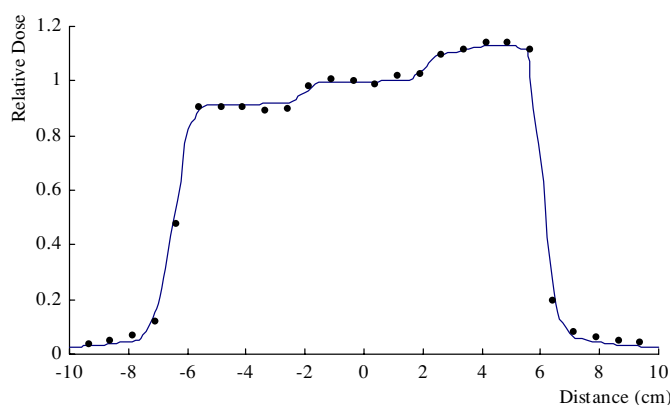
Figure 4. Comparison of the film (continuous line) with PXC (●) measurements for a *step* IMRT beam.

had a DTA of 0.18 cm. In the low-dose zone, the average difference was $1.6 \pm 1.1\%$, a value similar to that measured for the beam-profile tests. These results reproduce the behaviour obtained with static fields. As mentioned previously, the increase in the mean value of the difference may be caused by stray radiation interacting with the read-out electronics, but this hypothesis is to be further investigated.

These results show that PXC is well suited to measure these types of dynamic fields; indeed, more tests are needed to verify the behaviour with extreme dose distributions (e.g. bar pattern).

3.5. Dependence on leaf velocity

The response of the detector was studied as a function of the MLC leaf velocity in the range between 0.07 and 2 cm s^{-1}. The highest value was chosen as it corresponds to the maximum speed normally used at IRCC for therapy. The test was performed by measuring the charge collected by the central detector of the PXC for eight equally spaced leaf velocities. The delivered monitor units have been compared with the PXC response normalized to the slowest speed. The differences have a mean value of $0.6 \pm 0.7\%$ (1σ). The PXC charge collection time is approximately 0.5 ms, being the drift velocity of ions in air approximately 1 cm ms^{-1} (Knoll 2000). The rise time of the microelectronics chip read out has been discussed in Belletti *et al* (1999) and is below 10 ns. These results confirm that the time response of the detector-electronics ensemble is adequate for the 2 cm s^{-1} speed of MLC leaves.

3.6. Clinical IMRT verification

For clinical IMRT plans, the verification was performed on four different disease sites in the head and neck, with all IMRT fields checked for every plan. Figures 5 and 6 show a comparison between PXC and film measurement, and TPS calculation for field 5 of the chordoma plan.

The comparison of TPS, film and PXC is shown in table 3, where the percentages of pixels with $\gamma \leqslant 1$ are shown for each field. For each IMRT field, only pixels with a dose larger than 3% of the maximum have been taken into account. Considering all fields of the four pathologies, the number of pixels with $\gamma \leqslant 1$ was $97.7 \pm 0.5\%$ for PXC versus film and
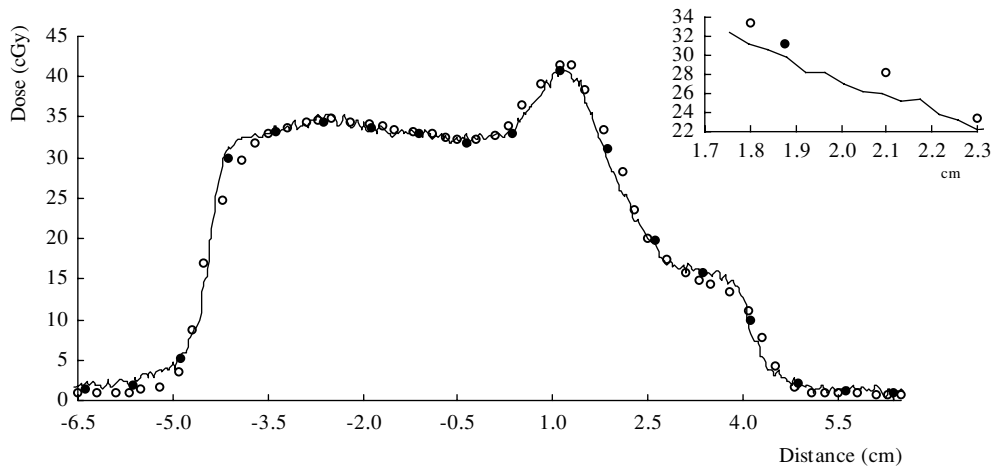
Figure 5. Cross-plane (*x*) profile for the central region (*y* = 3.75 mm) of field 5 of chordoma plan; the figure shows a comparison between TPS calculation (○), PXC (●) and film (continuous line) measurements. The inset shows details of the penumbra region, to evaluate the DTA; in this specific case, maximum DTA of PXC versus film for *x* profile is 0.08 cm.
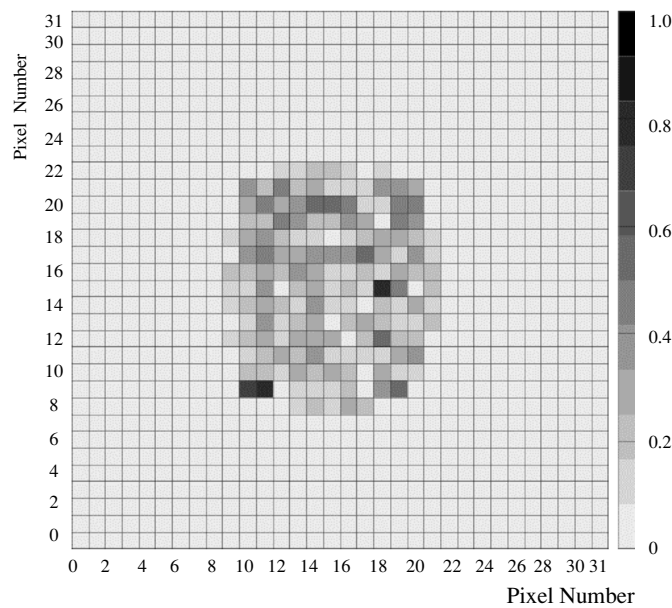

Figure 6. Example of the distribution of the γ parameter (PXC versus film) for the field shown in figure 5. The *x*- and *y*-axes show the pixel number (1–32).

97.6 ± 0.5% for PXC versus TPS. Two treatments (ethmoid and parotid) have more than 97% of points with $\gamma \leqslant 1$ for all fields, whereas chordoma and skull base feature several fields in the 93–97% range. Indeed, the dose distributions of the first two plans are homogeneous and confined to a small area; on the other hand, the latter have very irregular shapes.

Table 3. Summary of results, showing the maximum dose and the percentages of pixels with $\gamma \leqslant 1$ for each field; a 0.3 cm distance to agreement (DTA) and 3% dose difference relative to maximum dose of the field are used.

Pathology	Field #	Maximum dose (cGy)	Film–PXC $\gamma \leqslant 1$ (%)	TPS–PXC $\gamma \leqslant 1$ (%)
Cervical chordoma	1	43.3	94	96
	2	30.2	100	95
	3	39.4	100	98.5
	4	56.4	95	94
	5	42.8	100	98.5
	6	46.3	99	95
	7	39.7	88	93
Ethmoid	1	79.7	100	100
	2	55.2	100	100
	3	51.4	99	100
	4	51.2	100	100
Parotid	1	113.3	100	99
	2	46.3	99	100
	3	20.3	97	98.8
	4	34.5	97	98.6
Skull base	1	43.3	95	96
	2	43.8	98	99
	3	93.2	98	98
	4	92.5	96	95

It is a feature of IMRT fields to have several steep dose gradients. This implies that errors introduced in the dose measurement when using a detector that integrates on a finite size are of concern. To estimate this error as introduced by the PXC, we have used seven cervical chordoma fields; this specific plan was chosen because it is the one with the largest number of regions characterized by a large gradient. The assessment was done using two methods, both using data measured with a film positioned at 5 cm water-equivalent depth and scanned with a grid pitch of 0.042 cm.

In the first method, only film data were used. For each position (x) in the range between -8 and $+8$ cm with respect to the field central axis, data were integrated over an area equal to a PXC element (i.e. a circle with 0.4 cm diameter) centred around x. The result of this integration over the film area was subsequently compared with the point-like film measurement at each x. This way, it was possible to compare the *true* measurement of the film at a certain point with the measurement obtained when integration is introduced. The maximum absolute difference is 1.0 cGy, corresponding to 2.3% of the maximum dose for that field which was 42.8 cGy. Similar results have been obtained for the six remaining fields of the chordoma plan. This gives the estimate of the maximum error due to the integration, near the position where the gradient changes. The quoted result (1.0 cGy) includes a component of 0.5 cGy due to fluctuations on the film measurements.

In the second method, we compared the data taken with the PXC to the film measurements located at the centre of each pixel. Again, the difference is a function of the gradient and the maximum is 1.9 cGy, corresponding to 4.4% of the maximum dose for that field. The same comparison has been performed with DTA, obtaining an average value of 0.06 ± 0.08 cm and a maximum value of 0.13 cm.

4. Conclusions

A matrix of 1024 ionization chambers, the PiXel Chamber (PXC), has been tested to assess its ability to measure the clinical treatments with dynamic IMRT of head and neck cancers used at IRCC. First, a number of dosimetric characteristics were investigated: output factor, leaf-speed dependence, response versus dose rate, response to simple modulations (EDW and *step* IMRT). Then, a total of 19 clinical fields have been measured, comparing PXC measurements with TPS and film, using the γ-index method; the agreement between TPS and PXC was similar to the agreement obtained between film and TPS.

The PXC has been shown to be useful for IMRT pre-treatment QA, allowing the measurement of dose in several points with the advantages of an ionization chamber dosimeter. As a word of caution, the limited number of detectors and the dimension of a single detector have to be always kept in mind when dealing with very high gradient or very small field sizes. On the other hand, the PXC provides measurements of 0.07 cm^3 1024 ionization chambers on an active area of 24×24 cm^2 as often as every 0.5 ms.

Acknowledgment

References

Almond P R, Biggs P J, Coursey B M, Hanson W F, Huq M S, Nath R and Rogers D W O 1999 AAPM's TG-51 protocol for clinical reference dosimetry of high-energy photon and electron beams *Med. Phys.* **26** 1847–70

Amerio S *et al* 2004 Dosimetric characterization of a large area pixel-segmented ionisation chamber *Med. Phys.* **31** 414–20

Belletti S *et al* 1999 Performances of a pixel ionisation chamber with electron beams *Phys. Med.* **XV** 137–41

Bonazzola G C, Cirio R, Donetti M, Marchetto F, Mazza G, Peroni C and Zampieri A 1998 Performances of a VLSI wide dynamic range current-to-frequency converter for strip ionisation chambers *Nucl. Instrum. Methods Phys. Res.* A **405** 111–20

Bonin R *et al* 2004 A pixel chamber to monitor the beam performances in hadrontherapy *Nucl. Instrum. Methods Phys. Res.* A **519** 674–86

Bourhaleb F, Cirio R, Degiorgis P G, Donetti M, Marchetto F, Marletti M, Mazza G, Peroni C, Rizzi E and SanzFreire C 2002 Radiation damage studies of a recycling integrator VLSI chip for dosimetry and control of therapeutical beams *Nucl. Instrum. Methods Phys. Res.* A **482** 752–60

Brusasco C *et al* 1997 Strip ionisation chambers as 3D detector for hadrontherapy *Nucl. Instrum. Methods Phys. Res.* A **389** 499–512

Bucciolini M, Banci Buonamici F, Mazzocchi S, De Angelis C, Onori S and Cirrone G A P 2003 Diamond detector versus silicon diode and ion chamber in photon beams of different energy and field size *Med. Phys.* **30** 2149–54

Burch S E, Kearfott K J, Trueblood J H, Shieds W C, Yeo J I and Wang C K 1997 A new approach to film dosimetry for high energy photon beams: lateral scatter filtering *Med. Phys.* **24** 775–83

Capote R, Sanchez-Doblado F, Leal A, Lagares J I, Arrans R and Hartmann G 2004 An EGSnrc Monte Carlo study of the microionisation chamber for reference dosimetry of narrow irregular IMRT beamlets *Med. Phys.* **31** 2416–22

Convery D J and Rosembloom M E 1992 The generation of intensity modulated fields for conformal radiotherapy by dynamic multileaf collimation *Phys. Med. Biol.* **37** 1359–74

Ellis F, Hall E J and Oliver R 1959 A compensator for variations in tissue thickness for high energy beams *Br. J. Radiol.* **32** 421–2

Ezzell G A, Galvin J M, Low D, Palta J R, Rosen I, Sharpe M B, Xia P, Xiao Y, Xing L and Yu C X 2003 Guidance document on delivery, treatment planning, and clinical implementation of IMRT: report of the IMRT Subcommittee of the AAPM Radiation Therapy Committee *Med. Phys.* **30** 2089–115

Fraass B, Doppke K, Mutic S, Hunt M, Kutcher G, Starkschall G, Stern R and Van Dyke J 1998 American Association of Physicists in Medicine Radiation Therapy Committee Task Group 53: quality assurance for clinical radiotherapy treatment planning *Med. Phys.* **25** 1773–1829

Garelli E 2002 Analysis of data obtained with a pixel ionisation chamber used as dosimeter in conventional radiation therapy *Thesis* University of Torino, Italy (in Italian)

Greer P B and Popescu C 2003 Dosimetric properties of an amorphous silicon electronic portal imaging device for verification of dynamic intensity modulated radiation therapy *Med. Phys.* **30** 1618–27

ICRU Report 50 1993 Prescribing, recording, and reporting photon beam therapy

Jursinic P A and Nelms B E 2003 A 2D diode array and analysis software for verification of intensity modulated radiation therapy delivery *Med. Phys.* **30** 870–9

Khan F M 1994 *The Physics of Radiation Therapy* (Baltimore: Williams & Wilkins)

Knoll G F 2000 *Radiation Detection and Measurement* 3rd edn (New York: Wiley) 133 pp

Letourneau D, Gulam M, Yan D, Oldham M and Wong J W 2004 Evaluation of 2D diode array for IMRT quality assurance *Radiother. Oncol.* **70** 199–206

Leybovich L B, Sethi A and Dogan N 2003 Comparison of ionisation chambers of various volumes for IMRT absolute dose verification *Med. Phys.* **30** 119–23

Li J S, Boyer A L and Ma C-M 2001 Verification of IMRT dose distributions using a water beam imaging system *Med. Phys.* **28** 2466–74

Low D A, Harms W B, Mutic S and Purdy J A 1998 A technique for the quantitative evaluation of dose distributions *Med. Phys.* **25** 656–61

Low D A, Parikh P, Dempsey J F, Wahab S and Huq S 2003 Ionisation chamber volume averaging effects in dynamic intensity modulated radiation therapy beams *Med. Phys.* **30** 1706–11

Ma L, Geis P B and Boyer A L 1998 Quality assurance for dynamic multileaf collimator modulated fields using a fast beam imaging system *Med. Phys.* **25** 656–61

Martens C, De Wagter C and De Neve W 2000 The value of the Pin-Point ion chamber for characterization of small field segments in intensity-modulated radiotherapy *Phys. Med. Biol.* **45** 2519–30

Martens C, De Wagter C and De Neve W 2001 The value of the LA48 linear ion chamber array for characterization of intensity-modulated beams *Phys. Med. Biol.* **46** 1131–48

Moran J M, Roberts D A, Nurushev T S, Antonuk L E, El-Mohri Y and Fraass B A 2005 An active matrix flat panel dosimeter (AMFPD) for in-phantom dosimetric measurements *Med. Phys.* **32** 466–72

Olch A J 2002 Dosimetric performance of an enhanced dose range radiographic film for intensity modulated radiation therapy quality assurance *Med. Phys.* **29** 2159–68

Pasma K L, Dirkx M L P, Kroonwijk, Visser A G and Heijmen B J M 1999 Dosimetric verification of intensity modulated beams produced with dynamic multileaf collimation using an electronic portal imaging device *Med. Phys.* **26** 2373–8

Purdy J A (Chairman of Working Group) 2001 Intensity-modulated radiation therapy: current status and issues of interest *Int. J. Radiat. Oncol. Biol. Phys.* **51** 880–914

Rustgi S N and Frye D M D 1995 Dosimetric characterization of radiosurgical beams with a diamond detector *Med. Phys.* **22** 2117–21

Simon W E, Shi J and Iannello C A 2000 Wide field calibration of a multi-sensor array *United States Patent no* 6125335 (Assignee: Sun Nuclear Corporation, Melbourne, FL)

Stasi M, Baiotto B, Barboni G, Chauvie S, Emanuelli S, Rivolta A and Scielzo G 2003 Comparison of values of different ionisation chambers for characterization of small field segments used in intensity-modulated radiotherapy *Radiother. Oncol.* **68** (Suppl 1) S104

Stasi M, Baiotto B, Barboni G and Scielzo G 2004 The behavior of several micro-ionisation chambers in small IMRT fields *Med. Phys.* **31** 2792–5

Sykes J R, James H V and Williams P C 1999 How much dose film sensitivity increase at depth for larger field size? *Med. Phys.* **26** 329–30

Ting J Y and Davis L W 2001 Dose verification for patients undergoing IMRT *Med. Dosim.* **26** 205–13

Tsai J S, Wazer D E, Ling M N, Wu J K, Fagundes M, DiPetrillo T, Kramer B, Koistinen M and Engler M J 1998 Dosimetric verification of the dynamic intensity modulated radiation therapy of 92 patients *Int. J. Radiat. Oncol. Biol. Phys.* **40** 1213–30

Van Esch A, Depuydt T and Huyskens D P 2004 The use of an aSi-based EPID for routine absolute dosimetric pre-treatment verification of dynamic IMRT fields *Radiother. Oncol.* **71** 223–34

Warkentin B, Steciw S, Rathee S and Fallone B G 2003 Dosimetric IMRT verification with a flat-panel EPID *Med. Phys.* **30** 3143–55

Watts R J 1998 Evaluation of a diode detector array for use as a linear accelerator QC device *Med. Phys.* **25** 247–50

Webb S 1989 Optimization of conformal radiotherapy dose distribution by simulated annealing *Phys. Med. Biol.* **34** 1349–70

Webb S 1992 Optimization by simulated annealing of three-dimensional conformal treatment planning for radiation fields defined by a multileaf collimator: II. Inclusion of two-dimensional modulation of the x-ray intensity *Phys. Med. Biol.* **37** 1689–704

Webb S 1994 Optimization the planning of intensity-modulated radiotherapy *Phys. Med. Biol.* **39** 2229–46

Webb S 1997 *The Physics of Conformal Radiotherapy* (Bristol: Institute of Physics Publishing)

Webb S 2000 *Intensity Modulated Radiation Therapy* (Bristol: Institute of Physics Publishing)

Xing K, Curran B, Hill R, Holmes T, Ma L, Forster K and Boyer A L 1999 Dosimetric verification of a commercial inverse treatment planning system *Phys. Med. Biol.* **44** 463–78

Yeo J I and Wang C K 1997 A filtration method for improving film dosimetry in photon radiation therapy *Med. Phys.* **24** 1943–53

Zeidan O A, Li J G, Ranade M, Stell A M and Dempsey J F 2004 Verification of step-and-shoot IMRT delivery using a fast video-based electronic portal imaging device *Med. Phys.* **31** 463–76

Zhu T C, Ding L, Liu C R and Palta J R 1997 Performance evaluation of a diode array for enhanced dynamic wedge dosimetry *Med. Phys.* **24** 1173–80

Zhu X R, Jursinic P A, Grimm D F, Lopez F, Rownd J J and Gillin M T 2002 Evaluation of Kodak EDR2 film for dose verification of intensity modulated radiation therapy delivered by a static multileaf collimator *Med. Phys.* **29** 1687–92